Delft University of Technology

Wind load estimation on bridges using latent force models enriched with environmental data

Petersen, Oyvind W.; Øiseth, Ole; Lourens, E.

Wind load estimation on bridges using latent force models enriched with environmental data

Ø. W. Petersen [1]**, O. Øiseth** [1]**, E. Lourens** [2]
[1] NTNU, Department of Structural Engineering
e-mail: **oyvind.w.petersen@ntnu.no**

[2] TU Delft
2628 CD Delft, the Netherlands

Abstract

An application of inverse force identification of wind loads on bridges is presented. This contribution explores the extension of latent force models (LFMs) in Kalman filters. Specifically, it is shown how LFMs can be enriched with environmental information from wind data in order to realistically reflect the underlying physics behind the wind loads. This is demonstrated in a case study of a long-span suspension bridge equipped with a structural monitoring system, where an extensive data set of 103 time series of 30-minute events is used. The results show that the estimation of modal wind loads and modal response states is stable. Moreover, optimization of LFMs with maximum likelihood methods shows that optimized solutions match well with the actual (measured) wind load conditions. The work elevates the prospects of physics-informed LFMs with interpretable hyperparameters.

1 Introduction

One of the most engineering important tasks in the design of large civil structures is to validate the structural resistance to environmental loads. A considerable challenge is that the environmental loading has inherent uncertainties due to the stochastic behavior of natural processes such as wind and waves. Reducing the environmental load uncertainties is important in order to attain better estimates of the dynamic responses of bridges, tall buildings, and wind turbines.

As the deployment of structural health monitoring systems on critical civil structures is becoming more frequent, measured structural responses are available to engineers and researchers. In previous research, it has been widely studied the use of Kalman filter-based techniques for state and input estimation [1, 2, 3, 4, 5] , wherein the measured responses are used to inversely reconstruct the unknown loads and global response states of the structure. In more recent developments, the use of latent force models (LFMs) in input estimation was proposed [6]. This entails modeling the dynamic evolution of the unknown loads as random Gaussian processes that are characterized by tunable covariance (kernel) functions. This extension enables the encoding of prior information about the loading, such as load magnitude, smoothness, or frequency content. However, the choice of suitable covariance functions and tuning of LFM hyperparameters remains to be scrutinized.

This paper considers the encoding of physical information in the design of LFMs, with a focus on wind loading on bridges. It is recognized that state and input estimation is an intricate problem when confronted with limited data, sensor noise, model inaccuracies, and numerical instabilities in the system inversion. Thus, it could be advantageous to enrich the filters with environmental information in order to tune the solutions towards more realistic physical estimates. Such environmental information may consist of wind data, wave data, temperatures, load mechanisms, or any other prior information that pertains to the loads for the specific case.

It is shown how the LFMs can be designed based on realistic prior beliefs on the characteristics of the
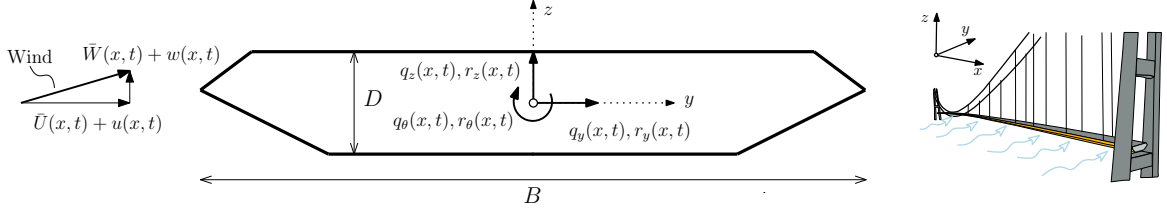
Figure 1: Strip model for buffeting loads acting on the bridge deck from incident wind. Wind velocities, loads, and responses all refer to a hypothetical center point of the bridge deck.

wind loads. An example implementation is presented using monitoring data from a long-span suspension bridge. The conjoined framework merges information from wind measurements, response (acceleration) measurements, numerical (finite elements) models, and wind tunnel tests in order to produce better data-based estimates of wind loads and modal response states of long-span bridges.

2   Theoretical framework

2.1   Linear models for turbulent wind loads on bridge decks

For non-extreme wind states, the wind loading on bridges is commonly modeled with linearized theory. In the following, a brief review of state-of-the-art theory for wind-induced buffeting response in bridges is presented. For more comprehensive explanations, we refer to books on the subject [7, 8]. The linear equation of motion for the structural response $\mathbf{r}(t)$ reads as follows:

$$\mathbf{M}_0\ddot{\mathbf{r}}(t) + (\mathbf{C}_0 - \mathbf{C}_{ae})\dot{\mathbf{r}}(t) + (\mathbf{K}_0 - \mathbf{K}_{ae})\mathbf{r}(t) = \mathbf{f}_b(t) \tag{1}$$

Here, $\mathbf{M}_0$, $\mathbf{C}_0$, and $\mathbf{K}_0$ are still-air structural matrices, while $\mathbf{C}_{ae}$ and $\mathbf{K}_{ae}$ are matrices accounting for aeroelastic effects (e.g. added aerodynamic damping in the presence of wind). The load vector $\mathbf{f}_b(t)$ contains the buffeting (fluctuating) forces which are distributed on the entire bridge span. Since the spectral power of turbulent wind is concentrated in the lower frequency range, wind-induced global responses in bridges are dominated by a limited number of vibration modes. This makes reduced-order modal models accurate for representing the observed response behavior. The reduction $\mathbf{r}(t) \approx \mathbf{\Phi}\mathbf{z}(t)$ is therefore introduced to Eq. (1), where the mode shape matrix $\mathbf{\Phi}$ containing n_m modes is calculated from the undamped eigenvalue problem considering still-air properties (i.e. $\mathbf{M}_0$ and $\mathbf{K}_0$). The generalized equation of motion then reads:

$$\tilde{\mathbf{M}}_0\ddot{\mathbf{z}}(t) + (\tilde{\mathbf{C}}_0 - \tilde{\mathbf{C}}_{ae})\dot{\mathbf{z}}(t) + (\tilde{\mathbf{K}}_0 - \tilde{\mathbf{K}}_{ae})\mathbf{z}(t) = \mathbf{\Phi}^T\mathbf{f}_b(t) \tag{2}$$

where the notation $\tilde{(\cdot)}$ denotes the generalized system matrices:

$$\tilde{\mathbf{M}}_0 = \mathbf{I}, \quad \tilde{\mathbf{C}}_0 = 2\mathbf{\Xi}_0\mathbf{\Omega}_0, \quad \tilde{\mathbf{K}}_0 = \mathbf{\Omega}_0^2 \tag{3}$$

where $\mathbf{\Omega}_0$ is diagonal with natural frequencies and $\mathbf{\Xi}_0$ is assumed diagonal with still-air damping ratios. To convert to state-space form, the modal state vector $\mathbf{x}(t) = [\mathbf{z}(t)^T \ \dot{\mathbf{z}}(t)^T]^T$ is introduced:

$$\dot{\mathbf{x}}(t) = \mathbf{A}_c\mathbf{x}(t) + \mathbf{B}_c\mathbf{p}(t) \tag{4}$$

$$\mathbf{A}_c = \begin{bmatrix} \mathbf{0} & \mathbf{I} \\ -\tilde{\mathbf{M}}^{-1}(\tilde{\mathbf{K}}_0 - \tilde{\mathbf{K}}_{ae}) & -\tilde{\mathbf{M}}^{-1}(\tilde{\mathbf{C}}_0 - \tilde{\mathbf{C}}_{ae}) \end{bmatrix}, \quad \mathbf{B}_c = \begin{bmatrix} \mathbf{0} \\ \tilde{\mathbf{M}}^{-1} \end{bmatrix} \tag{5}$$

In Eq. (4), we define $\mathbf{p}(t) = \mathbf{\Phi}^T\mathbf{f}_b(t)$ as the modal buffeting loads, which are discussed next. We refer to Fig. 1 for a concept illustration. In the well-established linearized models of wind loads due to turbulence,

the distributed buffeting forces acting on the bridge deck are given by [8]:

$$\begin{bmatrix} q_{\mathrm{b},y}(x,t) \\ q_{\mathrm{b},z}(x,t) \\ q_{\mathrm{b},\theta}(x,t) \end{bmatrix} = \frac{1}{2}\rho\bar{U}(x,t)B \begin{bmatrix} 2(D/B)\bar{C}_D & (D/B)C'_D - \bar{C}_L \\ 2\bar{C}_L & C'_L - (D/B)\bar{C}_D \\ 2B\bar{C}_M & BC'_M \end{bmatrix} \begin{bmatrix} u(x,t) \\ w(x,t) \end{bmatrix} \tag{6}$$

In compact matrix form, Eq. (6) reads:

$$\mathbf{q}_{\mathrm{b}}(x,t) = \mathbf{B}_{\mathbf{q}}(x)\mathbf{v}(x,t) \tag{7}$$

Thus, the loads are linear with respect to the alongwind and vertical turbulence components called $u(x,t)$ and $w(x,t)$. The other symbols are: the air density ρ; the mean alongwind velocity $\bar{U}(x,t)$; the mean vertical velocity $\bar{W}(x,t)$; the height D and width B of the bridge deck; the aerodynamic coefficients $\{\bar{C}_D, C'_D, \bar{C}_L, C'_L, \bar{C}_M, C'_M\}$ for drag, lift, and pitching moment. These six aerodynamic coefficients are specific for the bridge deck geometry (shape) and can be obtained from section model tests in wind tunnels.

The wind velocity along the entire bridge is a stationary stochastic field characterized by a two-point statistical description using the following cross-spectral density format:

$$\mathbf{S}_{\mathbf{vv}}(\omega, x_1, x_2) = \begin{bmatrix} S_{uu}(\omega, x_1, x_2) & S_{uw}(\omega, x_1, x_2) \\ S_{wu}(\omega, x_1, x_2) & S_{ww}(\omega, x_1, x_2) \end{bmatrix} \tag{8}$$

where the diagonal matrix element is defined as:

$$S_{mm}(\omega, x_1, x_2) = \sqrt{S_m(\omega, x_1)S_m(\omega, x_2)}C_{mm}(\omega, \Delta x), \quad m \in \{u, w\} \tag{9}$$

where $S_u(\omega)$ and $S_w(\omega)$ are single-point spectral densities, for which a Kaimal [9] (one-sided) spectral model is adopted:

$$\frac{S_m(f)f}{\sigma_u^2} = \frac{A_m \frac{fz}{\bar{U}}}{(1 + 1.5A_m \frac{fz}{\bar{U}})^{5/3}}, \quad m \in \{u, w\} \tag{10}$$

$C_{uu}(\omega, \Delta x)$ and $C_{ww}(\omega, \Delta x)$ are span-wise coherence functions where $\Delta x = |x_1 - x_2|$ is the span-wise distance between the two points. Here, the Davenport exponential model is used:

$$C_{mm}(\omega, \Delta x) = \exp\left(-K_m \frac{\omega \Delta x}{2\pi\bar{U}}\right), \quad m \in \{u, w\} \tag{11}$$

The cross-correlation between u and w is neglected: $S_{uw}(\omega, x_1, x_2) = 0$. In general, many other alternative spectral and coherence models could be used. However, the introduced Kaimal spectrum fits well with the wind conditions from the bridge in the case study presented later. This wind field model relies on spectral parameters A_u and A_w and coherence parameters K_u and K_w, which commonly are fitted from wind data or given assumed values when location-specific data is unavailable. The spectral density matrix for modal buffeting loads is obtained by integrating the buffeting forces along the whole span:

$$\mathbf{S}_{\mathbf{PP}}(\omega) = \int_0^L \int_0^L \boldsymbol{\Phi}_{\mathrm{ae}}(x_1)^{\mathrm{T}}\mathbf{B}_{\mathbf{q}}(x_1)\, \mathbf{S}_{\mathbf{vv}}(\omega, x_1, x_2)\, \mathbf{B}_{\mathbf{q}}(x_2)^{\mathrm{T}}\, \boldsymbol{\Phi}_{\mathrm{ae}}(x_2)\, \mathrm{d}x_1\, \mathrm{d}x_2 \tag{12}$$

where $\boldsymbol{\Phi}_{\mathrm{ae}}(x)$ is a matrix containing the modal values in the lateral (y), vertical (z), and pitching (θ) degrees of freedom (DOFs) of the box girder:

$$\boldsymbol{\Phi}_{\mathrm{ae}}(x) = \begin{bmatrix} \phi_y^{(1)}(x) & \dots & \phi_y^{(n_{\mathrm{m}})}(x) \\ \phi_z^{(1)}(x) & \dots & \phi_z^{(n_{\mathrm{m}}))}(x) \\ \phi_\theta^{(1)}(x) & \dots & \phi_\theta^{(n_{\mathrm{m}}))}(x) \end{bmatrix}, \quad x \in [0, L] \tag{13}$$

The corresponding cross-covariance matrix is calculated by the inverse Fourier transform:

$$\boldsymbol{\kappa}_{\mathbf{pp}}(\tau) = \int_{-\infty}^{\infty} \mathbf{S}_{\mathbf{pp}}(\omega) \exp(i\omega\tau) \, \mathrm{d}\omega \tag{14}$$

This completes the description of classic linear models for wind loading. We emphasize that the models presented in this section are based on assumed physical phenomena and empirical formulas. These models serve as a nominal basis for the loads in e.g. design and *forward* simulations. However, it is rarely expected that the models perfectly represent the real-life conditions due to their simplifications, linearizations, unmodelled physics, uncertain parameters, topographical influence, etc. In the next section, the *inverse* modeling of the load is introduced. This is, in contrast to the forward problem, a situation where the loads are treated as an unknown quantity that is eventually inversely estimated from response data.

2.2 Latent force models for inverse force identification

Latent force models (LFMs) in inverse force identification were proposed in [6]. LFMs has its foundation in the popular machine-learning tool Gaussian process (GP) regression [10], in which probabilistic inference is used on data-driven problems. In the context of force identification, the evolution of the input $p(t)$ is modelled as a random GP which is an output from a differential equation. Consider the following simple first-order differential equation LFM for a force component $p_j(t)$ $(j = 1, \ldots, \mathrm{n_m})$:

$$\dot{s}_j(t) = -\lambda_j s_j(t) + \tilde{w}_j(t) \tag{15}$$

$$p_j(t) = s_j(t) \tag{16}$$

The characteristics of the latent state $s_j(t)$ is dependent the time-scale (smoothness) parameter λ_j, as well as the variance of the white noise GP $\tilde{w}_j(t)$, denoted $\sigma_{\tilde{w},j}^2$. The output $p_j(t)$ is a zero mean GP with a stationary autocovariance function, which for the LFM in Eqs. (15)-(16) simply becomes becomes an exponential:

$$\kappa_{p,j}(\tau) = \mathbb{E}[p_j(t)p_j(t+\tau)] = \sigma_{p,j}^2 \exp(-\lambda_j|\tau|) \tag{17}$$

where the process variance is $\sigma_{p,j}^2 = \sigma_{\tilde{w},j}^2/(2\lambda_j)$. Eq. (17) is the well-known $\nu = 1/2$-Matérn kernel in GP regression. The spectral density of $p_j(t)$ is given by the Fourier transform:

$$S_{p,j}(\omega) = \frac{1}{2\pi} \int_{-\infty}^{\infty} \kappa_{p,j}(\tau) \exp(-i\omega\tau) \, \mathrm{d}\omega = \frac{\sigma_{\tilde{w},j}^2}{2\pi(\lambda_j^2 + \omega^2)} \tag{18}$$

Since multiple modal loads are present, the most straightforward option is to consider each modal load independently (neglecting cross-correlations). The LFM can then be constructed as a block-diagonal system:

$$\begin{bmatrix} \dot{s}_1(t) \\ \vdots \\ \dot{s}_{\mathrm{n_m}}(t) \end{bmatrix} = \begin{bmatrix} F_{\mathrm{c},1} & & \\ & \ddots & \\ & & F_{\mathrm{c},\mathrm{n_m}} \end{bmatrix} \begin{bmatrix} s_1(t) \\ \vdots \\ s_{\mathrm{n_m}}(t) \end{bmatrix} + \begin{bmatrix} L_{\mathrm{c},1} & & \\ & \ddots & \\ & & L_{\mathrm{c},\mathrm{n_m}} \end{bmatrix} \begin{bmatrix} \tilde{w}_1(t) \\ \vdots \\ \tilde{w}_{\mathrm{n_m}}(t) \end{bmatrix} \tag{19}$$

$$\begin{bmatrix} p_1(t) \\ \vdots \\ p_{\mathrm{n_m}}(t) \end{bmatrix} = \begin{bmatrix} H_{\mathrm{c},1} & & \\ & \ddots & \\ & & H_{\mathrm{c},\mathrm{n_m}} \end{bmatrix} \begin{bmatrix} s_1(t) \\ \vdots \\ s_{\mathrm{n_m}}(t) \end{bmatrix} \tag{20}$$

where $F_{\mathrm{c},j} = -\lambda_j$, $L_{\mathrm{c},j} = 1$, $H_{\mathrm{c},j} = 1$, and the subscript c denotes system matrices in continuous time. In compact matrix format, the total LFM is defined as:

$$\dot{\mathbf{s}}(t) = \mathbf{F}_{\mathrm{c}}\mathbf{s}(t) + \mathbf{L}_{\mathrm{c}}\tilde{\mathbf{w}}(t) \tag{21}$$

$$\mathbf{p}(t) = \mathbf{H}_{\mathrm{c}}\mathbf{s}(t) \tag{22}$$

The state-space format of the LFM allows it to be seamlessly fused together with vibration state-space models (Eq. 4), as shown in Section 2.3. The design of the LFMs and their hyperparameters is discussed in Sec. 3.

2.3 Augmented system formulation

The augmented state-space model is constructed by combining the vibration system in Eq. (4) and the LFM in Eqs. (21) and (22):

$$\begin{bmatrix} \dot{\mathbf{x}}(t) \\ \dot{\mathbf{s}}(t) \end{bmatrix} = \begin{bmatrix} \mathbf{A}_\mathrm{c} & \mathbf{B}_\mathrm{c}\mathbf{H}_\mathrm{c} \\ \mathbf{0} & \mathbf{F}_\mathrm{c} \end{bmatrix} \begin{bmatrix} \mathbf{x}(t) \\ \mathbf{s}(t) \end{bmatrix} + \begin{bmatrix} \mathbf{0} \\ \mathbf{L}_\mathrm{c}\tilde{\mathbf{w}}(t) \end{bmatrix} \tag{23}$$

or simply:

$$\dot{\mathbf{x}}_\mathrm{c}^\mathrm{a}(t) = \mathbf{F}_\mathrm{ac}\mathbf{x}_\mathrm{c}^\mathrm{a}(t) + \tilde{\mathbf{w}}_\mathrm{c}^\mathrm{a}(t) \tag{24}$$

The linear response output vector $\mathbf{y}(t)$, consisting of accelerations and/or displacements, is constructed as follows:

$$\mathbf{y}(t) = \mathbf{S}_\mathrm{acc}\ddot{\mathbf{r}}(t) + \mathbf{S}_\mathrm{disp}\mathbf{r}(t) \tag{25}$$

The corresponding state-space format reads:

$$\mathbf{y}(t) = \mathbf{G}_\mathrm{c}\mathbf{x}(t) + \mathbf{J}_\mathrm{c}\mathbf{p}(t) = \begin{bmatrix} \mathbf{G}_\mathrm{c} & \mathbf{J}_\mathrm{c}\mathbf{H}_\mathrm{c} \end{bmatrix} \begin{bmatrix} \mathbf{x}(t) \\ \mathbf{s}(t) \end{bmatrix} = \mathbf{H}_\mathrm{ac}\mathbf{x}_\mathrm{c}^\mathrm{a}(t) \tag{26}$$

where the following matrices are defined:

$$\mathbf{G}_\mathrm{c} = \begin{bmatrix} \mathbf{S}_\mathrm{disp}\boldsymbol{\Phi} - \mathbf{S}_\mathrm{acc}\boldsymbol{\Phi}\tilde{\mathbf{M}}^{-1}(\tilde{\mathbf{K}}_0 - \tilde{\mathbf{K}}_\mathrm{ae}) & -\mathbf{S}_\mathrm{acc}\boldsymbol{\Phi}\tilde{\mathbf{M}}^{-1}(\tilde{\mathbf{C}}_0 - \tilde{\mathbf{C}}_\mathrm{ae}) \end{bmatrix}, \quad \mathbf{J}_\mathrm{c} = \begin{bmatrix} \mathbf{S}_\mathrm{acc}\boldsymbol{\Phi} \end{bmatrix} \tag{27}$$

The system is discretized in time ($t_k = k\Delta t$). When stochastic noise is added both the state and output equation, Eqs. (23) and (26) now read as follows:

$$\mathbf{x}_{k+1}^\mathrm{a} = \mathbf{F}_\mathrm{ad}\mathbf{x}_k^\mathrm{a} + \mathbf{w}_k^\mathrm{a}, \quad \mathbf{x}_k^\mathrm{a} = [\mathbf{x}(t_k)^\mathrm{T}\ \mathbf{s}(t_k)^\mathrm{T}]^\mathrm{T} \tag{28}$$

$$\mathbf{y}_k = \mathbf{H}_\mathrm{ad}\mathbf{x}_k^\mathrm{a} + \mathbf{v}_k \tag{29}$$

Here, the subscript d denotes system matrices in discrete time, and the system matrices are defined as:

$$\mathbf{F}_\mathrm{ad} = \exp(\mathbf{F}_\mathrm{ac}\Delta t), \quad \mathbf{H}_\mathrm{ad} = \mathbf{H}_\mathrm{ac} \tag{30}$$

The covariances of the noise processes are given as follows [11]:

$$\mathbb{E}[\mathbf{v}_k\mathbf{v}_k^\mathrm{T}] = \mathbf{R} \tag{31}$$

$$\mathbb{E}[\mathbf{w}_k^\mathrm{a}\mathbf{w}_k^\mathrm{a}] = \mathbf{Q}_\mathrm{ad} = \int_0^{\Delta t} \exp\left(\mathbf{F}_\mathrm{ac}(\Delta t - \tau)\right)\mathbf{Q}_\mathrm{ac}\exp\left(\mathbf{F}_\mathrm{ac}(\Delta t - \tau)^\mathrm{T}\right)\mathrm{d}\tau + \begin{bmatrix} \mathbf{Q}_\mathrm{xd} & \mathbf{0} \\ \mathbf{0} & \mathbf{0} \end{bmatrix} \tag{32}$$

where we define:

$$\mathbf{Q}_\mathrm{ac} = \begin{bmatrix} \mathbf{0} & \mathbf{0} \\ \mathbf{0} & \mathbf{L}_\mathrm{c}\mathbf{Q}_{\tilde{w}\mathrm{c}}\mathbf{L}_\mathrm{c}^\mathrm{T} \end{bmatrix}, \quad \mathbf{Q}_{\tilde{w}\mathrm{c}} = \mathrm{diag}(\sigma_{\tilde{w}_1}^2, \sigma_{\tilde{w}_2}^2, \ldots, \sigma_{\tilde{w}_\mathrm{nm}}^2) \tag{33}$$

The integration term in Eq. (32) is related to the input dictated by the LFM. In order to account for a small amount of unmodelled dynamics or other noise on the states, there is also an added term $\mathbf{Q}_\mathrm{xd}$, which is typically considered a tuning parameter in Kalman filtering applications.

After the augmented state-space model is constructed, the sequence of measured response data $\{\mathbf{y}_1, \mathbf{y}_2, \ldots, \mathbf{y}_N\}$ is used in a classic Kalman filter (KF) [12] and subsequently a backward Rauch-Tung-Striebel (RTS) smoother [13] (see Eqs. (36)-(45) in the Appendix). After the filtering and smoothing, the augmented state $\hat{\mathbf{x}}_k^\mathrm{a}$ contains the modal state estimate $\hat{\mathbf{x}}(t)$ and modal load estimate $\hat{\mathbf{p}}(t) = \mathbf{H}_\mathrm{c}\hat{\mathbf{s}}(t)$. This can be used to estimate
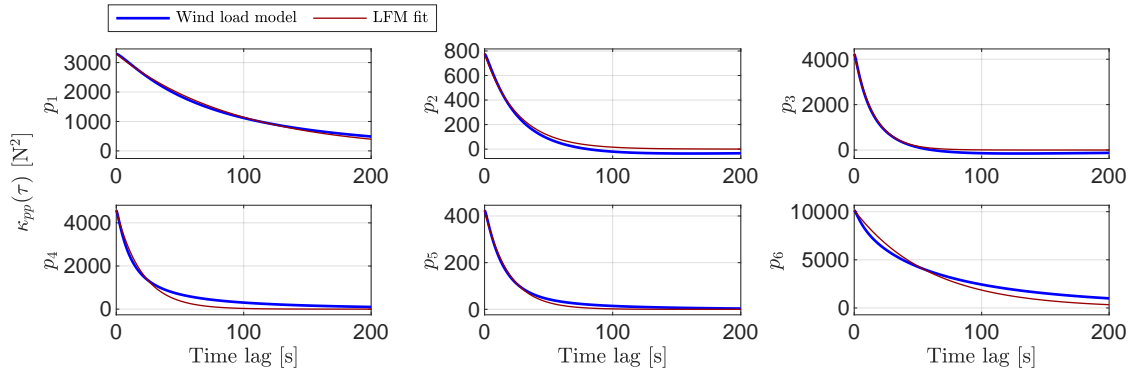
Figure 2: Covariance function of modal wind loads from wind load theory (Eq. (14)) and the LFM (Eq. (17)). Typical example shown for six modes.
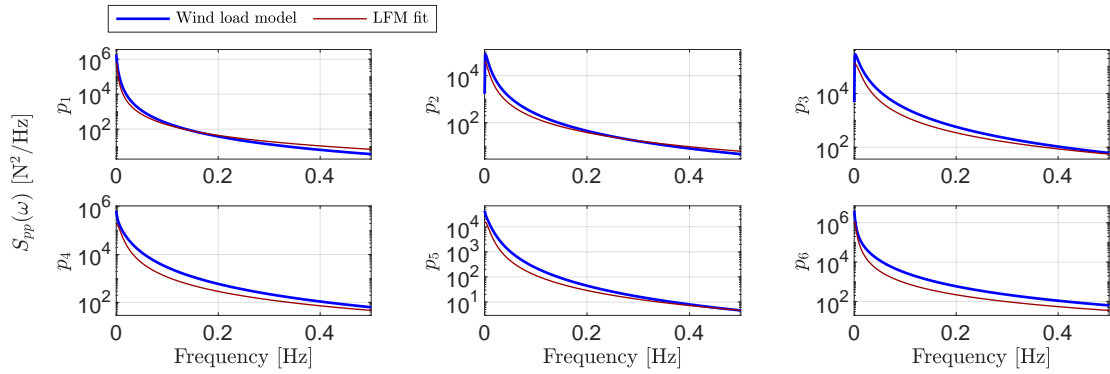

Figure 3: Spectral density of modal wind loads from wind load theory (Eq. (12)) and the LFM (Eq. (18)). Typical example shown for six modes.

responses in locations where there are no sensors (aka. virtual sensing):

$$\hat{\mathbf{y}}(t) = \begin{bmatrix} \mathbf{G}'_c & \mathbf{J}'_c \end{bmatrix} \begin{bmatrix} \hat{\mathbf{x}}(t) \\ \hat{\mathbf{p}}(t) \end{bmatrix} \tag{34}$$

where $\mathbf{G}'_c$ and $\mathbf{J}'_c$ needs to be constructed from Eq. (27) for the desired location and type of output.

3   Design of latent force models for wind loading

In principle, many other kernel types than Eq. (17) could be used to form the matrices $\mathbf{F}_c$, $\mathbf{L}_c$, and $\mathbf{H}_c$. Popular examples are higher-order Matérn kernels, periodic kernels, squared exponential kernels, or combinations of these [14, 15, 16, 17]. The kernel type and its hyperparameters should ideally be adapted to the specific case based on evidence support or engineering beliefs on the underlying structure of the output process under consideration. This work is limited to considering the exponential kernel in Eq. (17) due to its simplicity and prospects for representing buffeting loads. This is because the atmospheric turbulence, on the scales relevant for wind loading on bridges, is reasonably characterized by a slowly decaying covariance function (Fig. 2).

Next, the hyperparameters λ_j and $\sigma_{p,j}$ respectively controlling the smoothness and load magnitude must be quantified. The idea is to assign realistic values reflecting the underlying physics of the wind loading. This is accomplished by using the theoretical wind load model described in Sec. 2.1, which is utilized as a best initial guess for the wind load. Specifically, the LFM exponential kernel in Eq. (17) is fitted to the theoretical covariance function in Eq. (14). Here, a simple fitting procedure based on method of moments is performed to obtain λ_j and $\sigma_{p,j}$, see [18] for details. Representative examples for the case study presented later are
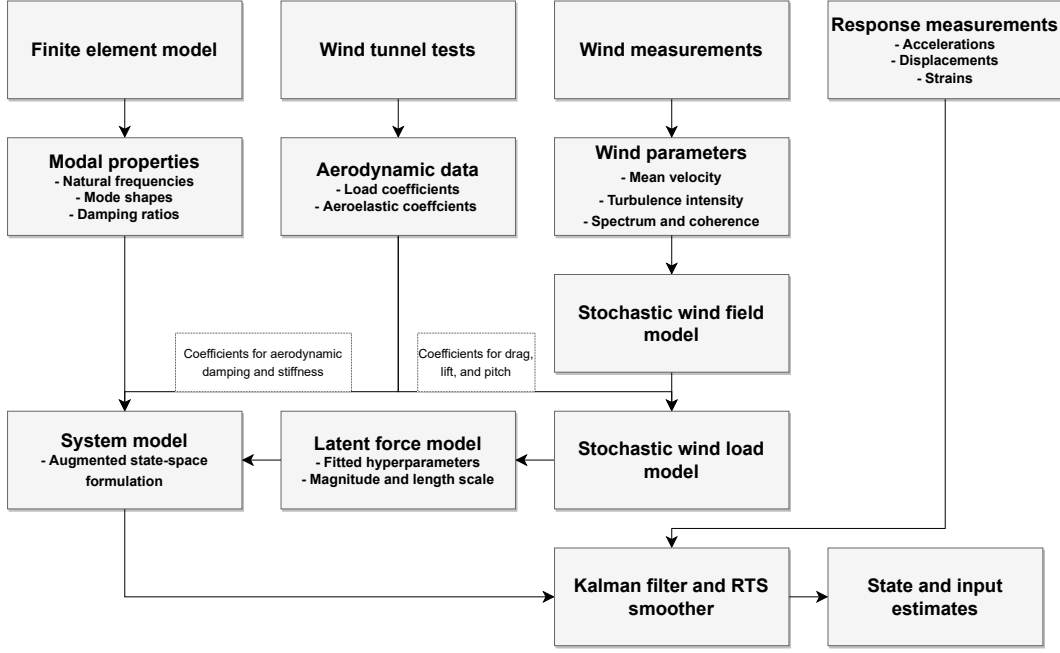
Figure 4: Overview of information sources and the steps in the analysis. Note that only acceleration output is available for the Hardanger bridge, although this can be combined with displacements or strains.

Table 1: Four different models used in the identification. The parameter optimization is based on Eq. (35).

Model No.	Mean wind velocity $\bar{U}$ [m/s]	Covariances	Wind field parameters $\{I_u, I_w, A_u, A_w, K_u, K_w\}$
#1	Fixed, from measured wind data	$\mathbf{R} = 10^{-6}\mathbf{I}$, $\mathbf{Q} = 10^{-1}\mathbf{I}$	Fixed, from measured wind data
#2	Optimized, $\in [5, 30]$	$\mathbf{R} = 10^{-6}\mathbf{I}$, $\mathbf{Q} = 10^{-1}\mathbf{I}$	Fixed, from measured wind data
#3	Optimized, $\in [5, 30]$	$\mathbf{R} = 10^{-7}\mathbf{I}$, $\mathbf{Q} = 10^{-1}\mathbf{I}$	Fixed, from measured wind data
#4	Optimized, $\in [5, 30]$	$\mathbf{R} = 10^{-7}\mathbf{I}$, $\mathbf{Q} = \mathbf{I}$	Fixed, from measured wind data

shown in Fig. 2 and 3 in the time and frequency domain, respectively. As expected, the fit is not perfect, but the exponential kernel is seemingly quite suitable for the purpose. Its simple and scalar state-space form (Eq. (15)) also makes it attractive.

This form of LFM design is a prior belief based on physical wind load models that are enriched with environmental data (parameters derived from measured wind velocities). However, this belief need not be an exact stochastic description of the wind load since the estimation of the states and loads in the Kalman filter heavily relies on the measured response data as well, in which the "true" wind loading conditions always are contained. See Fig. 4 for an overview of how the different informative data sources are fused together in the proposed framework.

In addition to obtaining hyperparameters by fitting them to physical wind load models, we also attempt other forms of optimization. One popular way to tune a hyperparameters set $\boldsymbol{\theta}$ is to maximize the likelihood of $p(\mathbf{y}_{[1:N]}|\boldsymbol{\theta})$, where the objective function is given by the following expression [19]:

$$\log(L) = -\frac{1}{2}\sum_{k=1}^{N}\left(\log(|\mathbf{S}_k|) + \mathbf{e}_k^T \mathbf{S}_k^{-1}\mathbf{e}_k\right) \tag{35}$$

where $\mathbf{S}_k$ is the covariance matrix of the innovation vector $\mathbf{e}_k$ in the Kalman filter; see Eqs. (36) and (37).

We explore four different LFM configurations that are summarized in Tab. 1, all with a link to wind load physics. The first (#1) is a nominal model solely using the wind data, without considering optimization of

Figure 5: The Hardanger Bridge.

Eq. (35). In the remaining three system models (#2, #3, #4), $\bar{U}$ is used as a tunable optimization parameter. In addition, several values for covariances $\mathbf{R}$ and $\mathbf{Q}_{xd}$ are used. As will be shown, this choice is made because the objective function in Eq. (35) is, to some extent, sensitive to the noise magnitudes.

4 Implementation for the Hardanger Bridge

4.1 Monitoring data, structural model, and aeroelastic model

The long-span suspension Hardanger Bridge (Fig. 5, $L = 1310$ m) is used as a case study. Its monitoring system consists of 20 triaxial accelerometers and 9 anemometers. For brevity, the monitoring system is not shown here, and we refer to previous works for details [18, 20, 21]. The measured data is also openly available in an online repository described in [21].

A total of n_y=24 acceleration signals in the lateral and vertical direction are used in the output $\mathbf{y}(t)$. The accelerometers at the mid-span of the bridge are held out for verification purposes. Results in this paper are shown for a batch of 103 data sets of 30-minute events from $22^{\text{nd}} - 26^{\text{th}}$ December 2016, a period with strong winds and winter storms.

The finite element model of the bridge is described in [18, 22]. In this paper, global $n_m = 15$ vibration modes are included in the reduced-order model. The natural frequencies range from 0.05 Hz to 0.4 Hz, and the still-air damping ratios are set to 0.5% proportional damping. The aeroelastic model, contributing mainly to increased aerodynamic damping $\mathbf{C}_{\text{ae}}$ (and a small aerodynamic stiffness $\mathbf{K}_{\text{ae}}$), is described in [18] and is based on theory from [23].

4.2 Processing of wind data

The wind data is processed in a series of steps in order to establish the parameters in the wind field model. For each of the 103 data sets, the following is performed:

(i) For each anemometer, the *moving* mean wind velocity $\bar{U}(t)$ is first found by sliding a 600 s (10 minutes) averaging window through the time series. The turbulence $u(t)$ is then defined as the fluctuation around the moving mean. As a necessary simplification, the mean wind velocity is hereafter adopted as a stationary constant ($\bar{U}$) equal to the average of $\bar{U}(t)$. The same procedure is repeated for the vertical direction to obtain $w(t)$. Examples are shown in Fig. 6.
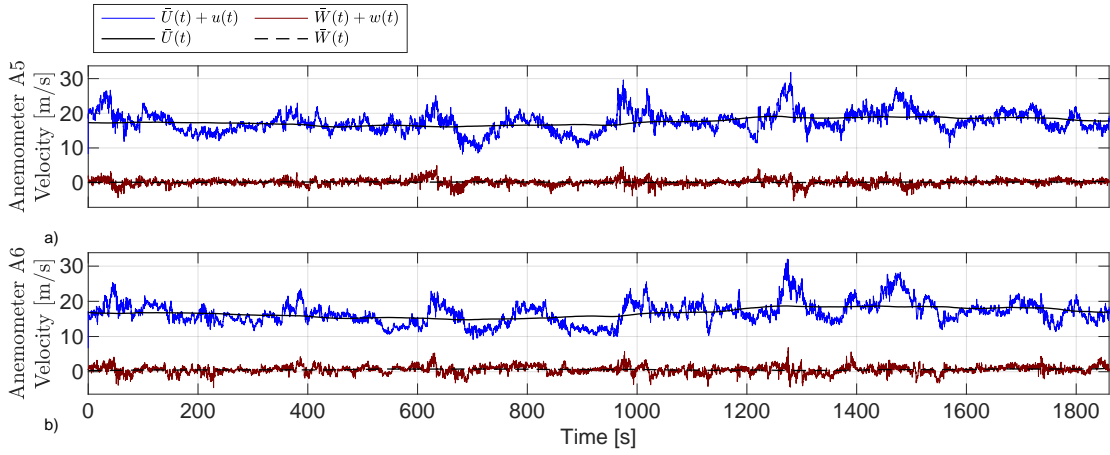
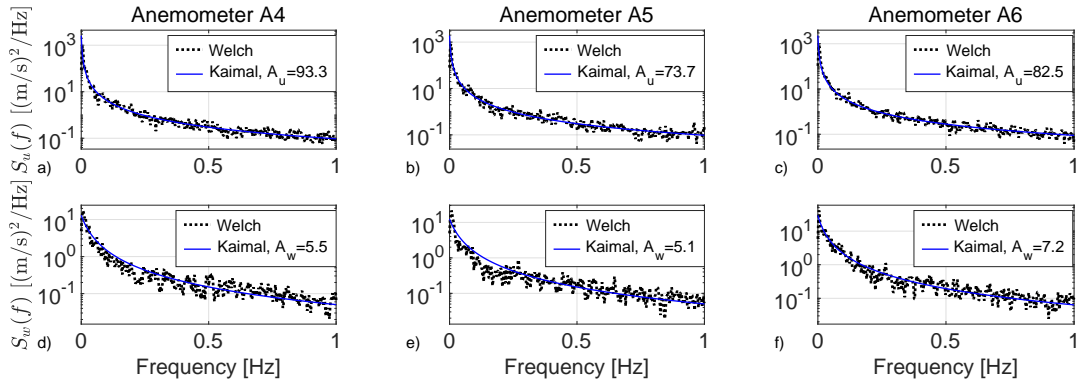Figure 6: Example of wind velocity data, and it decomposition into moving mean and turbulence components.

Figure 7: Example of fit of Kaimal spectrum to measured turbulence spectrum.

(ii) The standard deviation of $u(t)$ is found directly from the data as σ_u. The turbulence intensity is $I_u = \sigma_u/\bar{U}$. When repeated for the vertical direction, one obtains σ_w and $I_w = \sigma_w/\bar{U}$.

(iii) The auto spectral density of $u(t)$ for all anemometers is estimated by Welch's method. The Kaimal spectrum (Eq. (10)) is fitted to the Welch auto spectra to obtain the parameter A_u. The same procedure is repeated for the vertical direction to obtain A_w. Examples are shown in Fig. 7.

(iv) The cross-spectral density of $u(t)$ for all anemometers is estimated by Welch's method. The exponential coherence (Eq. (11)) is fitted to the Welch cross spectra to obtain the parameter K_u. The same procedure is repeated for the vertical direction to obtain K_w. This is not shown here for brevity; examples can be seen in [18].

(v) Several values for the wind field parameters $\{\bar{U}, I_u, I_w, A_u, A_w, K_u, K_w\}$ are now available since data from multiple anemometers are used. In order to obtain one uniform value for the entire span, an averaging operation is performed. This involves first a trim where the largest and smallest value is discarded to reduce the effect of outliers; then the mean value is taken.

The resulting wind parameter values for the 103 data sets are shown in Fig. 8 and Fig. 9. The figures unsurprisingly also reveal some variability within one data set. This indicates weak inhomogeneity (e.g. differences in mean wind velocities between anemometers) or uncertainty related to the processing (e.g. estimation of wind spectrum), and highlights the complexity in characterizing wind conditions for large structures. Nevertheless, both homogeneity and stationarity are implicitly assumed for the final wind field model. The black circles in Fig. 8 and Fig. 9 show the adopted (trimmed mean) values used in the final wind field models. Note that each data set (corresponding to a 30-minute event), is treated with its own wind field model since the environmental conditions are unique to that event.
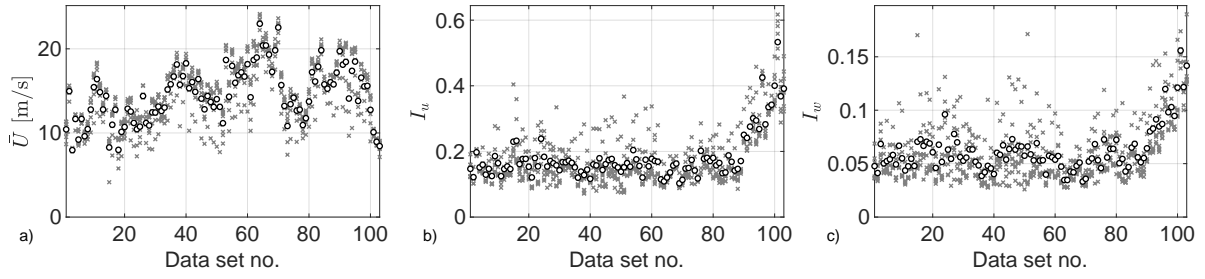
Figure 8: Mean wind velocities and turbulence intensities from the measured wind data. The black circles show the (trimmed) mean values, and the grey crosses are single data points.
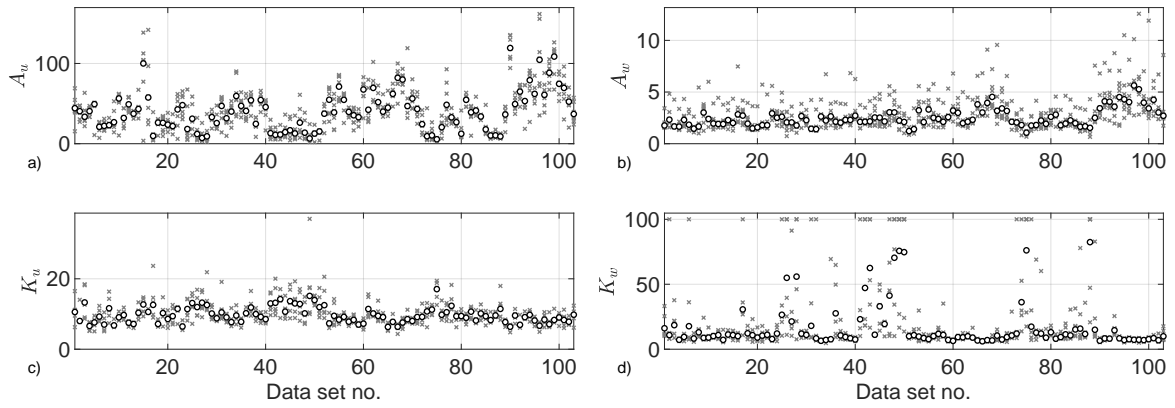

Figure 9: Kaimal spectral parameters and coherence decay parameters from the measured wind data. The black circles show the (trimmed) mean values, and the grey crosses are single data points.

After the wind field parameters are determined, it is straightforward to establish the stochastic the wind field model (Eq. (8)) and the then stochastic (modal) load model (Eq. (12)). Examples of resulting spectral densities have already been shown in Fig. 3. The aerodynamic load coefficients pertaining to the bridge deck of the Hardanger bridge are listed in Tab. 2.

4.3 State and input estimation with optimized parameters

Each data set is processed with its four different configured system models (Tab. 1), including the maximum likelihood estimation. The optimization results for the parameter $\bar{U}$ is shown in Fig. 10. Some interesting observations can be made: for system model #3 (red line), the optimized $\bar{U}$ follows the measured mean wind speeds (black line) very closely. This is an indication that the Kalman filter (fed with acceleration data) clearly prefers a tuned LFM that is rooted in the real physics of wind loads. The other two system models #2 and #4 (blue and green lines) generally yield slightly lower and slightly higher values than the measured wind velocities but generally follow the same trend. Note that the remaining wind field parameters $\{I_u, I_w, A_u, A_w, K_u, K_w\}$ are not optimized but kept as fixed values determined from the wind data processing procedure in Sec. 4.2.

As announced earlier, the optimization results also depend on the noise covariances. These covariances also regulate the extent to which the excitation load is explained as white noise rather than wind loads controlled by LFMs. We also point out that our experience is that the noise covariances also need to compensate for small but non-negligible model errors, for instance on the modal parameters in the system. Despite these facets, Fig. 10 reveals that the underlying physics of the wind load is reflected in optimized values for $\bar{U}$ used in the LFMs. Overall, we believe the optimization results are promising for the prospects of physics-informed LFMs with interpretable parameters. The extent to which it is desired that LFMs strictly represent

Table 2: Bridge deck dimensions in full scale, and linearized load coefficients for drag, lift, and pitching moment for the Hardanger Bridge wind tunnel tests.

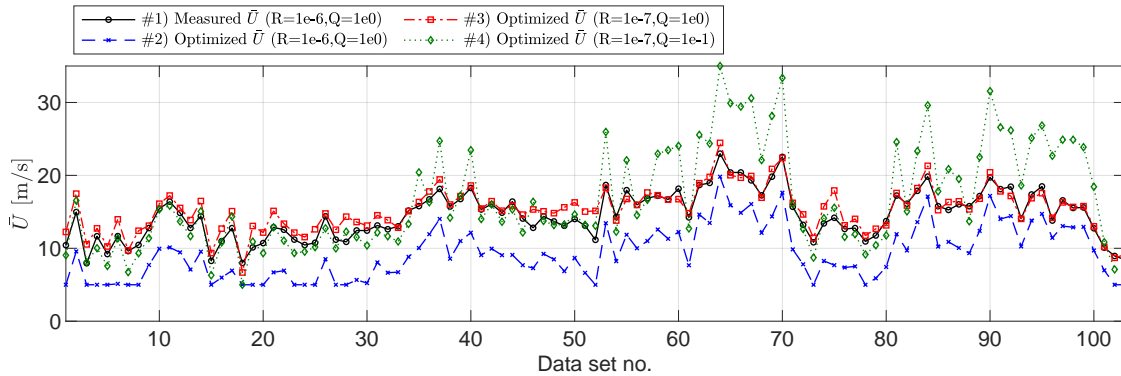| Geometry	Value	Drag coeff.	Value	Lift coeff.	Value	Pitch coeff.	Value
B	18.3 m	$\bar{C}_D$	0.850	$\bar{C}_L$	-0.382	$\bar{C}_M$	0
D	3.25 m	C'_D	1.389	C'_L	2.929	C'_M	0.903

Figure 10: Mean wind velocities: measured values and optimized values for different values of magnitude noise covariances.

one-to-one physics is also debatable since some of their strength lies in flexibility; nevertheless, interpretable parameters serve as good indicators of realism.

While results from all 103 data sets cannot be shown here, typical results for the state estimate are shown in Fig. 11. It is clearly noted that the state estimates are very similar for the four models, except for differences related to quasi-static behavior. Quasi-static responses are definitely present for wind-sensitive bridges, however, they are not well characterized by accelerometer data. The effect of this is visible for the displacement estimate at the bridge mid-span obtained from Eq. (34), which is shown in Fig. 12. The lateral displacements are prone to slow drift; a simple high-pass filter post-processing would remove this effect, but it is not performed here. For the vertical displacement and torsional pitching rotation, all models yield similar and, importantly, stable estimates.

Examples of time histories and spectral densities for selected modal loads are shown in Fig. 13 and Fig. 14. In general, there are greater differences in modal forces between system models than for the modal states, highlighting the complexities in the inverse identification of forces. Well-educated choices of covariance matrices are also a relevant topic but not studied in greater detail here. Although direct verification of the estimated loads is not feasible, it is promising that the spectral densities in Fig. 14 are largely similar to the nominal prediction from wind load models. The frequency-decaying nature in the spectral densities is clearly visible, except for the lower frequency range of the loads, which is not well characterized with acceleration output only.

5 Conclusions

In this paper, a framework for inverse wind load estimation on bridges was presented. It was proposed to use physics-designed LFMs in Kalman filters that are enriched with environmental wind data. Using a data set from the Hardanger bridge, the application was tested for a large data set. Through optimization, it was shown that the LFMs clearly reflect specific wind loading conditions, increasing the prospects of interpretable LFMs.

The methodology can join engineering information from wind tunnel tests, monitoring systems with wind and acceleration sensors, and finite element models to contribute to better estimates of global dynamic loading and responses of long-span bridges.
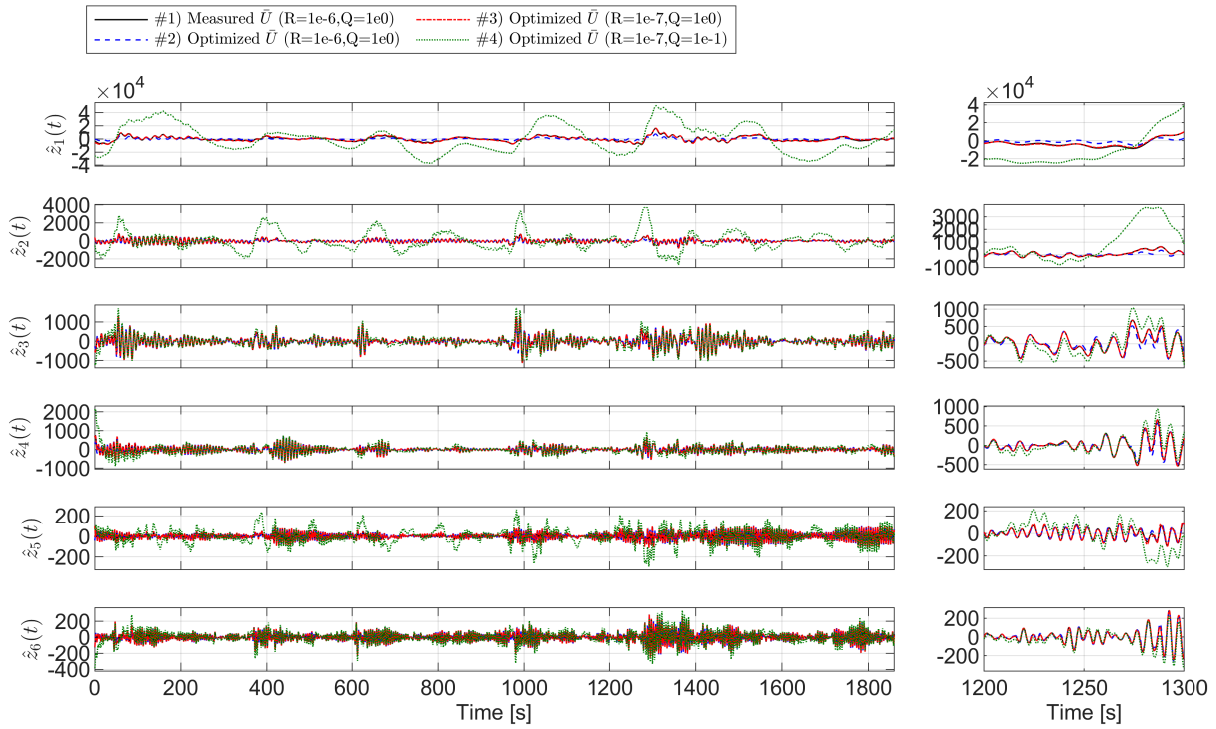
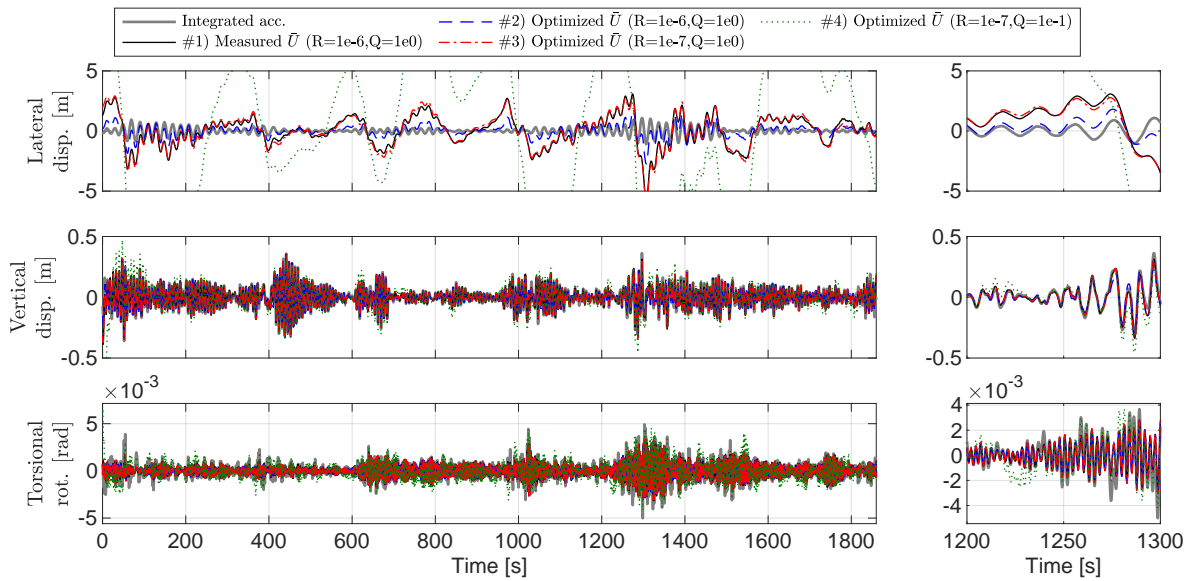Figure 11: Estimated modal states for six modes.

Figure 12: Estimated displacements at the mid-span compared to displacements obtained from integrated accelerations.
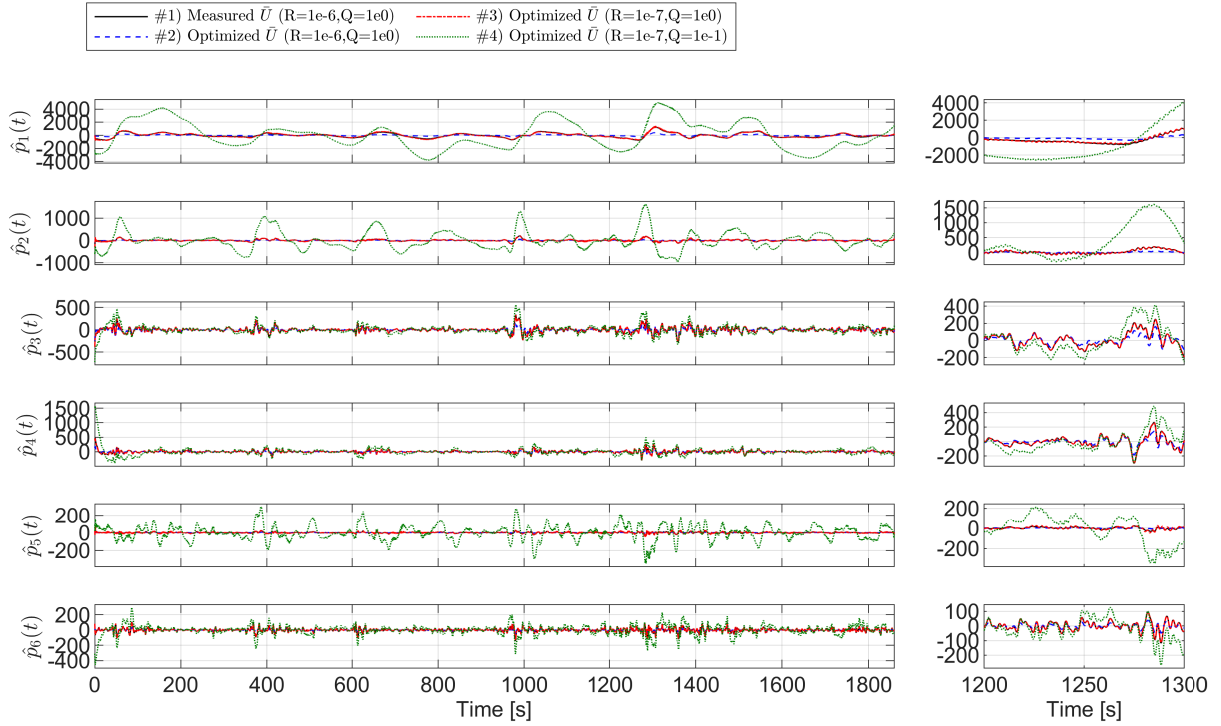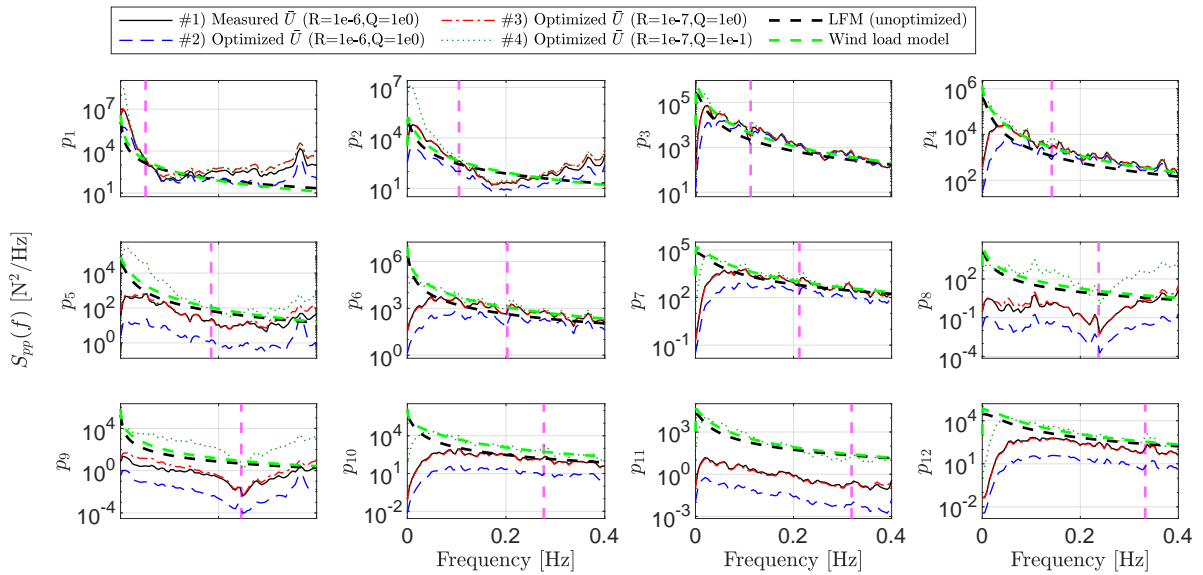
Figure 13: Estimated modal loads for six modes.

Figure 14: Spectral density of estimated modal loads by Welch's method for twelve modes shown together with the spectral density of the wind load model (Eq. (12)) and the LFM (Eq. (18)) (prior to optimization). The pink vertical lines indicate the respective modal natural frequencies.

References

[1] S. E. Azam, E. Chatzi, and C. Papadimitriou, "A dual Kalman filter approach for state estimation via output-only acceleration measurements," *Mechanical Systems and Signal Processing*, vol. 60, pp. 866–886, 2015.

[2] E. Lourens, C. Papadimitriou, S. Gillijns, E. Reynders, G. De Roeck, and G. Lombaert, "Joint input-response estimation for structural systems based on reduced-order models and vibration data from a limited number of sensors," *Mechanical Systems and Signal Processing*, vol. 29, pp. 310–327, 2012.

[3] E. Lourens, E. Reynders, G. De Roeck, G. Degrande, and G. Lombaert, "An augmented Kalman filter for force identification in structural dynamics," *Mechanical Systems and Signal Processing*, vol. 27, pp. 446–460, 2012.

[4] K. Maes, S. Gillijns, and G. Lombaert, "A smoothing algorithm for joint input-state estimation in structural dynamics," *Mechanical Systems and Signal Processing*, vol. 98, pp. 292–309, 2018.

[5] O. Sedehi, C. Papadimitriou, D. Teymouri, and L. S. Katafygiotis, "Sequential Bayesian estimation of state and input in dynamical systems using output-only measurements," *Mechanical Systems and Signal Processing*, vol. 131, pp. 659–688, 2019.

[6] R. Nayek, S. Chakraborty, and S. Narasimhan, "A Gaussian process latent force model for joint input-state estimation in linear structural systems," *Mechanical Systems and Signal Processing*, vol. 128, pp. 497–530, 2019.

[7] A. Kareem and A. Tamura, *Advanced structural wind engineering*.   Springer, 2015.

[8] E. Strømmen, *Theory of bridge aerodynamics*.   Springer Science & Business Media, 2010.

[9] J. C. Kaimal, J. Wyngaard, Y. Izumi, and O. Coté, "Spectral characteristics of surface-layer turbulence," *Quarterly Journal of the Royal Meteorological Society*, vol. 98, no. 417, pp. 563–589, 1972.

[10] C. E. Rasmussen, *Gaussian processes in machine learning*.   MIT Press, 2006.

[11] S. Särkkä *et al.*, *Recursive Bayesian inference on stochastic differential equations*.   Helsinki University of Technology, 2006.

[12] R. E. Kalman, "A new approach to linear filtering and prediction problems," *Journal of basic Engineering*, vol. 82, no. 1, pp. 35–45, 1960.

[13] H. E. Rauch, F. Tung, and C. T. Striebel, "Maximum likelihood estimates of linear dynamic systems," *AIAA journal*, vol. 3, no. 8, pp. 1445–1450, 1965.

[14] A. Solin and S. Särkkä, "Explicit link between periodic covariance functions and state space models," in *Artificial Intelligence and Statistics*.   PMLR, 2014, pp. 904–912.

[15] A. Solin and S. Särkkä, "Gaussian quadratures for state space approximation of scale mixtures of squared exponential covariance functions," in *2014 IEEE International Workshop on Machine Learning for Signal Processing (MLSP)*.   IEEE, 2014, pp. 1–6.

[16] S. Reece, S. Roberts, S. Ghosh, A. Rogers, and N. R. Jennings, "Efficient state-space inference of periodic latent force models," *Journal of Machine Learning Research*, vol. 15, pp. 2337–2397, 2014.

[17] M. A. Alvarez, D. Luengo, and N. D. Lawrence, "Linear latent force models using Gaussian processes," *IEEE transactions on pattern analysis and machine intelligence*, vol. 35, no. 11, pp. 2693–2705, 2013.

[18] Ø. W. Petersen, O. Øiseth, and E. Lourens, "Wind load estimation and virtual sensing in long-span suspension bridges using physics-informed Gaussian process latent force models," *Mechanical Systems and Signal Processing*, vol. 170, p. 108742, 2022.

[19] S. Särkkä, *Bayesian filtering and smoothing*. Cambridge University Press, 2013, vol. 3.

[20] A. Fenerci, O. Øiseth, and A. Rønnquist, "Long-term monitoring of wind field characteristics and dynamic response of a long-span suspension bridge in complex terrain," *Engineering Structures*, vol. 147, pp. 269–284, 2017.

[21] A. Fenerci, K. A. Kvåle, Ø. W. Petersen, A. Rønnquist, and O. Øiseth, "Dataset for long-term wind and acceleration monitoring of the Hardanger Bridge," *Journal of Structural Engineering*, vol. 147, no. 5, 2021.

[22] Ø. W. Petersen and O. Øiseth, "Finite element model updating of a long span suspension bridge," in *Proceedings of the International Conference on Earthquake Engineering and Structural Dynamics*, R. Rupakhety, S. Olafsson, and B. Bessason, Eds. Springer International Publishing, 2019, pp. 335–344.

[23] O. Øiseth, A. Rönnquist, and R. Sigbjörnsson, "Simplified prediction of wind-induced response and stability limit of slender long-span suspension bridges, based on modified quasi-steady theory: a case study," *Journal of Wind Engineering and Industrial Aerodynamics*, vol. 98, no. 12, pp. 730–741, 2010.

Appendix: Equations for Kalman filter and RTS smoother

The equations for the Kalman filter and RTS smoother are given below. Here, the notation $\hat{\mathbf{x}}^{\mathrm{a}}_{k|l}$ is the estimated augmented state at time step k using output data up to time step l; the associated error covariance matrix is $\hat{\mathbf{P}}^{\mathrm{a}}_{k|l}$. The estimate of the initial state in the first step, $\hat{\mathbf{x}}^{\mathrm{a}}_{1|0}$, is set to zero.

Kalman filter, measurement update ($k = 1, 2, \ldots, N$):

$$\mathbf{e}_k = \mathbf{y}_k - \mathbf{H}_{\mathrm{ad}}\hat{\mathbf{x}}^{\mathrm{a}}_{k|k-1} \tag{36}$$

$$\mathbf{S}_k = \mathbf{H}_{\mathrm{ad}}\mathbf{P}^{\mathrm{a}}_{k|k-1}\mathbf{H}^{\mathrm{T}}_{\mathrm{ad}} + \mathbf{R} \tag{37}$$

$$\mathbf{K}_k = \mathbf{P}_{k|k-1}\mathbf{H}^{\mathrm{T}}_{\mathrm{ad}}\mathbf{S}^{-1}_k \tag{38}$$

$$\hat{\mathbf{x}}^{\mathrm{a}}_{k|k} = \hat{\mathbf{x}}^{\mathrm{a}}_{k|k-1} + \mathbf{K}_k\mathbf{e}_k \tag{39}$$

$$\mathbf{P}^{\mathrm{a}}_{k|k} = \mathbf{P}^{\mathrm{a}}_{k|k-1} - \mathbf{K}_k\mathbf{S}_k\mathbf{K}^{\mathrm{T}}_k \tag{40}$$

Kalman filter, time update:

$$\hat{\mathbf{x}}^{\mathrm{a}}_{k+1|k} = \mathbf{F}_{\mathrm{ad}}\hat{\mathbf{x}}^{\mathrm{a}}_{k|k} \tag{41}$$

$$\mathbf{P}^{\mathrm{a}}_{k+1|k} = \mathbf{F}_{\mathrm{ad}}\mathbf{P}^{\mathrm{a}}_{k|k}\mathbf{F}^{\mathrm{T}}_{\mathrm{ad}} + \mathbf{Q}_{\mathrm{ad}} \tag{42}$$

Rauch-Tung-Striebel smoother, backward pass ($k = N, N-1, \ldots, 1$):

$$\mathbf{N}_k = \mathbf{P}^{\mathrm{a}}_{k|k}\mathbf{F}^{\mathrm{T}}_{\mathrm{ad}}(\mathbf{P}^{\mathrm{a}}_{k+1|k})^{-1} \tag{43}$$

$$\hat{\mathbf{x}}^{\mathrm{a}}_{k|N} = \hat{\mathbf{x}}^{\mathrm{a}}_{k|k} + \mathbf{N}_k(\hat{\mathbf{x}}^{\mathrm{a}}_{k+1|N} - \hat{\mathbf{x}}^{\mathrm{a}}_{k+1|k}) \tag{44}$$

$$\mathbf{P}^{\mathrm{a}}_{k|N} = \mathbf{P}^{\mathrm{a}}_{k|k} + \mathbf{N}_k(\mathbf{P}^{\mathrm{a}}_{k+1|N} - \mathbf{P}^{\mathrm{a}}_{k+1|k})\mathbf{N}^{\mathrm{T}}_k \tag{45}$$